New Dihexadecyldithiophosphate SAMs on Gold Provide Insight into the Unusual Dependence of Adsorbate Chelation on Substrate Morphology in SAMs of Dialkyldithiophosphinic Acids

ARTICLE *in* JOURNAL OF THE AMERICAN CHEMICAL SOCIETY · SEPTEMBER 2013

Impact Factor: 12.11 · DOI: 10.1021/ja404798q · Source: PubMed

6 AUTHORS, INCLUDING:

Muhammad Iqbal
University of Texas at Austin
14 PUBLICATIONS **124** CITATIONS
SEE PROFILE

S. Holger Eichhorn
University of Windsor
56 PUBLICATIONS **669** CITATIONS
SEE PROFILE

Charles Macdonald
University of Windsor
103 PUBLICATIONS **2,017** CITATIONS
SEE PROFILE

Tricia Breen Carmichael
University of Windsor
36 PUBLICATIONS **1,761** CITATIONS
SEE PROFILE

JACS
JOURNAL OF THE AMERICAN CHEMICAL SOCIETY

Article

pubs.acs.org/JACS

New Dihexadecyldithiophosphate SAMs on Gold Provide Insight into the Unusual Dependence of Adsorbate Chelation on Substrate Morphology in SAMs of Dialkyldithiophosphinic Acids

Ronan R. San Juan, Christopher J. Allan, Muhammad Iqbal, S. Holger Eichhorn, Charles L. B. Macdonald,* and Tricia Breen Carmichael*

University of Windsor, 401 Sunset Ave., Windsor, Ontario, Canada, N9B 3P4

Supporting Information

ABSTRACT: We report the formation and characterization of new self-assembled monolayers (SAMs) formed from dihexadecyldithiophosphate $(C_{16})_2$DDP and compare their properties with those of SAMs formed from the structurally similar adsorbate dihexadecyldithiophosphinic acid $(C_{16})_2$DTPA. The new $(C_{16})_2$DDP SAMs were characterized using X-ray photoelectron spectroscopy, reflection−absorption infrared spectroscopy, contact angle measurements, and electrochemical impedance spectroscopy. The data indicate that $(C_{16})_2$DDP forms SAMs on gold films formed by e-beam evaporation in which all adsorbates chelate to gold, in contrast to $(C_{16})_2$DTPA SAMs, in which 40% of the adsorbates are monodentate. The alkyl chains of the $(C_{16})_2$DDP SAM are also less densely packed and ordered than those of the $(C_{16})_2$DTPA SAM. To understand these differences, we present density functional theory calculations that show that there are only minimal differences between the geometric and electronic structures of the two adsorbates and that the energetic difference between monodentate and bidentate binding of a gold(I) ion are surprisingly small for both adsorbates. This study leads to the conclusion that differences in intermolecular interactions within the SAM are the driving force for the difference in chelation between the two adsorbates.

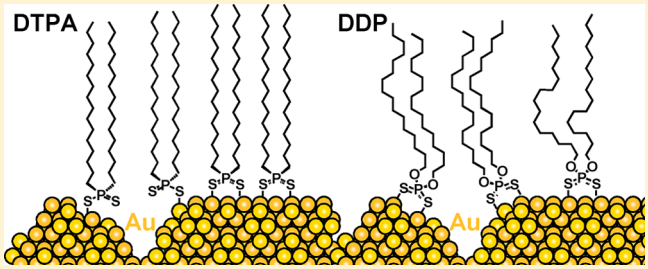

INTRODUCTION

Forming self-assembled monolayers (SAMs) is a widespread method to create surfaces with specific interfacial properties, such as wettability, friction, adhesion, biocompatibility, electrochemistry, and surface chemical reactivity.[1] In particular, SAMs of *n*-alkanethiolates on coinage metal surfaces have assisted and influenced a very wide range of scientific fields, from corrosion prevention[2−8] to molecular electronics[9−21] to biosensors.[1,22,23] Despite their impact in basic research, the main drawback with *n*-alkanethiolate SAMs is their limited stability to thermal[24−26] or electrochemical[27−30] desorption, which restricts their use in practical applications. In response to this problem, researchers have pioneered a new field in basic SAM research using chelating adsorbates to form SAMs.[31] The chelate effect has long been exploited in inorganic synthesis to produce new metal complexes with unique geometries and reactivities.[32] The key is the enhanced thermodynamic stability brought on by the use of chelating ligands instead of monodentate ligands. The chelate effect imparts this additional stability due to the more favorable entropy change that occurs upon binding a multidentate ligand compared to analogous monodentate ligands. By designing new chelating adsorbates, research groups have applied the chelate effect to surface science and produced SAMs that better withstand harsh conditions, such as elevated temperatures and the application of an electric potential.[26,30,31]

It seems straightforward that bidentate adsorbates should form SAMs in which all adsorbates chelate to the surface due to the thermodynamic stabilization from the chelate effect. There are numerous SAMs formed from bidentate adsorbates in the literature that support this assumption. Examples include a variety of chelating dithiols,[33−38] trithiols,[26,39−44] spiroalkanedithiols,[26,42,45−51] dithiocarbamates,[52−57] and dithiocarboxylic acids.[58−60] Dialkyldithiophosphinic acids ($R_2P(S)SH$, R_2DTPA) (Scheme 1a) are a class of chelating molecules that are distinct from this group: Our previous work has shown that, surprisingly, chelation of these adsorbates to gold surfaces can be disrupted due to the morphology of the gold film.[61] On gold films deposited by electron-beam evaporation, (As-Dep gold), the dense network of grain boundaries with depths ∼10 nm disrupts chelation of R_2DTPA molecules (R = hexyl, decyl, dodecyl, tetradecyl, hexadecyl).[62] The resulting SAMs are composed of a mixture of monodentate and chelating adsorbates. Chelation likely occurs on the small, atomically flat areas on the tops of the gold grains that measure ∼50 nm across. This hypothesis is supported by a study of $(C_{16})_2$DTPA SAMs formed on smooth, template-stripped (TS) gold surfaces, which consist of large, flat gold grains that measure

Received: May 13, 2013
Published: September 24, 2013

dx.doi.org/10.1021/ja404798q | J. Am. Chem. Soc. 2013, 135, 15784−15793

Scheme 1. Structures of (a) $(C_{16})_2$DTPA and (b) $(C_{16})_2$DDP

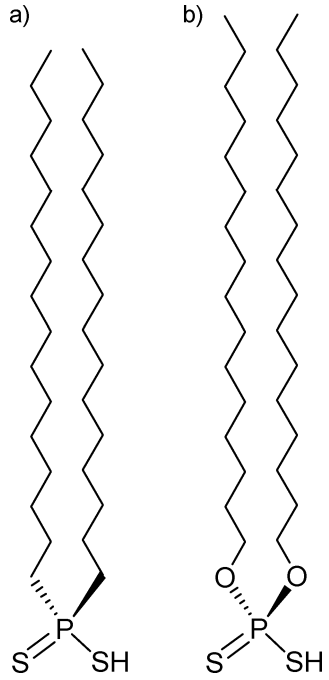

~200−500 nm across and are separated by shallow (~2 nm) grain boundaries. On TS gold, all $(C_{16})_2$DTPA adsorbates chelate to the surface.[61] The extent of chelation within R_2DTPA SAMs on As-Dep and TS gold also affects the organization of the alkyl chains,[61,62] R_2DTPA adsorbates that chelate to the gold surface are anchored at two points, which prevents rotation about the Au−S bonds and fixes the Au−S−P bond angles. For $(C_{16})_2$DTPA SAMs on TS gold, the tetrahedral geometry at phosphorus prevents the alkyl chains from packing closely, inhibiting van der Waals interactions between them and making the layer disordered and loosely packed. In contrast, the monodentate R_2DTPA molecules present in SAMs on As-Dep gold are anchored by a single point, which imparts some conformational flexibility to these adsorbates due to rotation about the Au−S bond and small changes in the Au−S−P bond angle. This conformational freedom allows the molecules to pack more densely within the SAM, enabling van der Waals interactions between alkyl chains that impart crystallinity to the alkyl layer.

Our work indicates that the morphology of the metal substrate is an important influence on the structure of R_2DTPA SAMs. Potential effects of substrate morphology on other SAMs have largely been overlooked in the literature, with the notable exception of molecular junction studies.[16] In this field, molecular junctions formed from *n*-alkanethiolates on flat, TS Ag substrates exhibit more reproducible junction-to-junction current densities and higher junction yields than molecular junctions formed on As-Dep Ag. The difference is due to fewer defective regions in *n*-alkanethiolate SAMs on flat TS Ag substrates. Although flatter substrates lead to "better" (i.e., more ordered) SAMs for *n*-alkanethiolates,[63,64] our work on R_2DTPA SAMs shows that the effect of substrate morphology on SAM structure may not easily be predicted for more complex adsorbates. The possibility of unexpected effects of substrate morphology on SAM structure is particularly important as increasingly complex adsorbates, including chelating adsorbates, are investigated in molecular junctions.[56,65−67]

In this paper, we address a key question: Why is chelation of R_2DTPA adsorbates disrupted by the morphology of the gold substrate, while this effect has not been reported for SAMs formed from other chelating adsorbates? One possibility is that the steric bulk of the R_2DTPA adsorbate due to the tetrahedral geometry at phosphorus hinders its ability to chelate in the deep grain boundaries of the As-Dep gold surface. This possibility seems unlikely, however, since SAMs formed from a variety of spiroalkanedithiols,[26,42,45−51] which have a similar shape, chelate fully to As-Dep gold surfaces. Furthermore, altering the steric demands of the alkyl groups in R_2DTPA adsorbates by changing the chain length has negligible impact on the percentage of chelating adsorbates in the SAM.[62] There are two other possible reasons for the dependence of binding mode of R_2DTPA adsorbates on gold morphology: First, the reason could be that the flexibility of the R_2DTPA adsorbate limits its ability to chelate the As-Dep gold surface. For example, the S−P−S bite angle may be too constrained to allow chelation across the atomic steps that make up the deep grain boundaries on As-Dep gold. Second, there could be an electronic effect unique to R_2DTPA adsorbates. To determine which factor controls the binding of R_2DTPAs, we report new SAMs formed from dihexadecyldithiophosphate [$(C_{16})_2$DDP] (Scheme 1b) on As-Dep gold and compare their properties with those of $(C_{16})_2$DTPA SAMs on As-Dep gold. Both R_2DTPA and R_2DDP molecules with short alkyl substituents (*i*-Bu_2DTPA,[68,69] *i*-$Amyl_2$DDP[70] and (*p*-fluorophenyl)$_2$DDP[71]) are used industrially as selective collectors for the flotation separation of precious metals from sulfide ores and only differ in the presence of oxygen atoms between the alkyl substituents and phosphorus in $(C_{16})_2$DDP. We show that this seemingly small structural difference—a single oxygen atom—between otherwise identical adsorbates fundamentally affects how the adsorbates bind to As-Dep gold. We present X-ray photoelectron spectroscopic data that reveals that $(C_{16})_2$DDP forms SAMs on As-Dep gold in which *all* adsorbates chelate to the gold surface. We use reflection−absorption infrared spectroscopy, contact angle measurements, and electrochemical impedance spectroscopy to show that the difference in the percentage of chelated adsorbates in $(C_{16})_2$DDP and $(C_{16})_2$DTPA SAMs is accompanied by differences in the organization of the alkyl chains and the electrochemical barrier properties. We furthermore present density functional theory (DFT) calculations that show that despite the observed experimental differences between the two SAMs, the optimized structures of the two adsorbates and their electronic structures are nearly identical. There is, however, a surprisingly small energetic difference between monodentate binding and chelation that leads us to conclude that low-energy differences in intermolecular interactions within the SAM are an important contributor to the difference in chelation between the two adsorbates. This work reveals that the self-assembly process for SAMs with S−P−S headgroups is complex and likely depends on the interplay between adsorbate−substrate interactions, intermolecular interactions, and substrate morphology.

■ EXPERIMENTAL SECTION

All chemicals were purchased commercially and used as received. Anhydrous diethyl ether and toluene were obtained from an Innovative Technologies solvent purification system. Nuclear magnetic resonance (NMR) spectroscopic data were obtained and recorded on

dx.doi.org/10.1021/ja404798q | J. Am. Chem. Soc. 2013, 135, 15784−15793

a Bruker Avance 300 MHz or a Bruker Avance 300 MHz Ultrashield at room temperature, and shifts are reported in parts per million (ppm). $^{31}P\{^1H\}$ NMR spectra were referenced externally to 85% H_3PO_4 (δ = 0 ppm). ^1H NMR spectra were referenced to residual proton peaks of $CDCl_3$ (δ = 7.27 ppm). $^{13}C\{^1H\}$ NMR spectra were referenced to $CDCl_3$ (δ = 77.0 ppm).

Synthesis of $(C_{16})_2$DDP. $(C_{16})_2$DDP was synthesized as described by Gümgüm et al.[72] with modifications: The microwave irradiation step was omitted. Instead, we heated excess 1-hexadecanol to 60 °C, to which we added P_4S_{10} slowly over a period of 30 min, and the reaction mixture was left stirring overnight. $(C_{16})_2$DDP was synthesized as a white solid in 89% yield. ^{31}P, ^1H, and ^{13}C NMR spectra are provided in Figure S1.

$(C_{16}H_{33}O)_2P(S)SH$: $^{31}P\{^1H\}$ NMR ($CDCl_3$, 121 MHz, 298 K): δ 79.6. ^1H NMR ($CDCl_3$, 300 MHz, 298 K): 4.25−4.14 (m, 4H, OCH_2), 1.76−1.69 (m, 4H, CH_2), 1.26 (m, CH_2), 0.87 (t, $|^3J_{H-H}|$ = 6.27 Hz, 6H, CH_3). $^{13}C\{^1H\}$ NMR ($CDCl_3$, 126 MHz, 298 K): δ 69.2 (s, OCH_2), 32.1 (s, CH_2), 29.8−29.4 (m, CH_2), 25.7 (s, CH_2), 22.8 (s, CH_2), 14.2 (s, CH_3).

Synthesis of $(C_{16})_2$DTPA. $(C_{16})_2$DTPA was synthesized as described by Miller et al.[61]

Gold Substrate Preparation and SAM Formation. Gold films were produced by the deposition of 2 nm of titanium as an adhesion promoter onto silicon wafers, followed by 200 nm of gold, using an electron-beam evaporator. Approximately 2 × 2 cm gold substrates were immersed into a 1 mM solution of $(C_{16})_2$DDP in anhydrous toluene or a 1 mM solution of $(C_{16})_2$DTPA in anhydrous toluene for 24 h. Substrates were then removed from solution, rinsed with anhydrous toluene, and dried under a stream of nitrogen.

Atomic Force Microscopy (AFM). AFM images were obtained using a Digital Instruments Multimode atomic force microscope run in contact mode. Veeco type silicon tip on nitride lever (SNL) cantilevers were used with a nominal tip radius of 2 nm and a nominal force constant of 0.12 N/m. The back side of each cantilever was coated with 45 ± 5 nm of Ti/Au. AFM images were collected over a 1 × 1 μm scan area using a scan rate of 1 Hz and a scanning resolution of 256 samples/line. Images were collected using Nanoscope 6 software and processed using WSxM 5.0 Develop 1.0 software.[73]

X-ray Photoelectron Spectroscopy (XPS). XPS spectra of $(C_{16})_2$DDP SAMs were collected at Surface Science Western (London, Ontario, Canada) using a Kratos Axis Nova X-ray photoelectron spectrometer with a monochromatic Al Kα source. The detection limit of the instrument is 0.1−0.5 at. %. Both survey-scan and high-resolution analyses were carried out over a 300 × 700 μm scan area. Survey-scan analyses were carried out with a pass energy of 160 eV, and high-resolution analyses were carried out with a pass energy of 20 eV. Samples were analyzed at a 30° takeoff angle (60° tilt). High-resolution sulfur line shapes were fit using two pairs of spin−orbit split components ($2p_{3/2}$ and $2p_{1/2}$) assuming a Gaussian/Lorentzian (70%:30%) line shape and a fixed splitting energy of 1.18 eV with a 2:1 area ratio.[74]

Infrared Spectroscopy. Reflection−absorption infrared (RAIR) spectra of $(C_{16})_2$DDP SAMs were collected using a Bruker IFS 66/v spectrometer equipped with a mercury cadmium telluride (MCT) detector and Harrick Autoseagull accessory. The p-polarized light was incident at 85° from the surface normal, and 1024 scans were collected at a resolution of 2 cm^{-1}.

Contact Angle Measurements. Advancing water and hexadecane contact angles of $(C_{16})_2$DDP SAMs were measured with a Ramé-Hart contact angle goniometer equipped with a microlitre syringe and a tilting stage. In each case, at least three drops from each of three samples were averaged.

Electrochemical Impedance Spectroscopy (EIS). EIS spectra of $(C_{16})_2$DDP and $(C_{16})_2$DTPA SAMs were collected using a BAS-Zahner IM6 ex impedance unit. A glass cell equipped with a calomel/saturated KCl reference electrode and a 1.0 mm Pt wire counter electrode was clamped to the working electrode, a 0.95 cm^2 area of the SAM on gold, and then filled with an aqueous solution of 1 mM $K_3Fe(CN)_6$, 1 mM $K_4Fe(CN)_6{\cdot}3H_2O$, and 10 mM Na_2SO_4. The measurements were made at an open-circuit potential set at ∼420 mV with a 5 mV ac perturbation that was controlled from 50 mHz to 200 kHz. The current response was measured, which is normalized to the area of the working electrode. The impedance data were fitted with an appropriate circuit model to provide values for the resistance and the capacitance of the SAM.

DFT Calculations. All DFT calculations were performed using the B3PW91 method implemented in the Gaussian 09 program suite[75] using the SHARCNET high-performance computing network (www.sharcnet.ca). Where applicable, the Stuttgart group (SDD) effective core potentials (ECP)[76,77] and corresponding basis sets were used for gold atoms and the 6-31+G(d) basis set was used for all lighter atoms in all calculations. Natural bond order (NBO)[78] analyses to determine orbital contributions, Wiberg Bond Indices and HOMO/LUMO energies were obtained using the NBO routine included in the Gaussian distributions. All stationary points were confirmed to be minima exhibiting no imaginary frequencies. The model anions DDP′ and DTPA′ were calculated with C_2 symmetry. Molecular orbital pictures and electrostatic potential plots were calculated using Molden.[79] Molecular orbital diagrams were generated using POV-Ray for Windows.[80] Proton and gold(I) ion affinities were calculated using energies in the following formula: affinity = $\Delta E^{elec}_{Rxn}\Delta E^{elec}_{Rxn}$ − ΔZPE + 5/2RT, where ΔE^{elec}_{Rxn} is the change in the electronic energy upon reaction (at 298.15 K); ΔZPE is the change in zero point energy; R = 8.314 J mol^{-1} K^{-1} and T = 298.15 K.

RESULTS

SAM Formation. We synthesized $(C_{16})_2$DDP and $(C_{16})_2$DTPA according to literature procedures[61,72] and then prepared SAMs by immersing gold-coated wafers prepared by e-beam evaporation into 1 mM solutions of the adsorbates anhydrous toluene for 24 h. The substrates were then removed from solution, rinsed with anhydrous toluene, and dried under a stream of nitrogen. To minimize surface contamination, As-Dep gold films were used immediately after removal from the e-beam evaporator to form SAMs. The morphology of these gold substrates was identical to the As-Dep gold substrates used in our studies of R_2DTPA SAMs.[61,62] The gold surface consisted of grains with an average size of ∼50 nm, separated by boundaries as deep as ∼8−10 nm and had a root-mean-square roughness of 27 Å (Figure 1). This roughness value was calculated using data collected over a 1 × 1 μm area of the gold substrate.

Binding of P(S)(SH) Headgroups to Gold. XPS analysis of $(C_{16})_2$DDP SAMs indicates that all $(C_{16})_2$DDP adsorbates chelate to the gold substrate, in contrast to $(C_{16})_2$DTPA SAMs, which contain 40% monodentate adsorbates.[62] Survey scans of the $(C_{16})_2$DDP SAM detected carbon, oxygen, phosphorus, sulfur, and gold, consistent with SAM formation (Figure S3). Previous high-resolution XPS (HR-XPS) studies of sulfur-containing SAMs on gold have established that the electronic environment of the sulfur atom and the nature of the interaction between sulfur and gold surface atoms influences the S 2p binding energies: The S $2p_{3/2}$ peaks of sulfur atoms bound to gold appear at binding energies of ∼161−162 eV, sulfur atoms that are not interacting with the gold surface give S $2p_{3/2}$ peaks at binding energies of ∼163−165 eV, and oxidized sulfur species give S $2p_{3/2}$ peaks at binding energies >166 eV.[81,82] The HR-XPS S 2p scans of $(C_{16})_2$DDP SAM (Figure 2) showed a line shape that we fit using one pair of S $2p_{3/2}$ and S $2p_{1/2}$ spin−orbit split components by assuming a Gaussian/Lorentzian (70%:30%) line shape and a splitting energy fixed at 1.18 eV.[74] The S $2p_{3/2}$ peak at 161.7 eV can be assigned to a sulfur species chemisorbed to gold. The presence of only this peak indicates that $(C_{16})_2$DDP adsorbates in the SAM all chelate to the gold surface. In comparison, HR-XPS analysis of

dx.doi.org/10.1021/ja404798q | J. Am. Chem. Soc. 2013, 135, 15784−15793

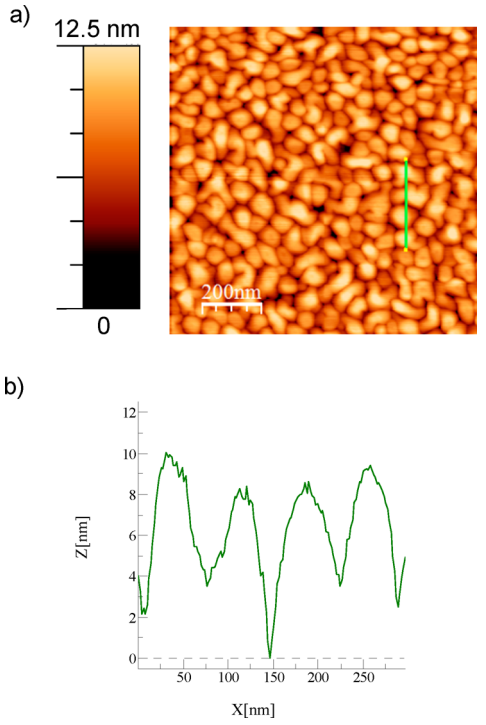

Figure 1. (a) AFM topographic image recorded in contact mode of the As-Dep gold film. (b) Cross-sectional profile corresponding to the green line in part (a).

the S 2p region of $(C_{16})_2$DTPA SAMs (Figure 2b) showed a complex line shape that was fit using two pairs of spin−orbit-split components (S $2p_{3/2}$ and S $2p_{1/2}$). The S $2p_{3/2}$ peaks appear at binding energies of 161.9 and 163.4 eV, which correspond to sulfur chemisorbed to gold and noninteracting sulfur, respectively. The integrated atomic ratio of the chemisorbed:noninteracting peaks was 80:20, which indicates that the SAM contains both bidentate and monodentate $(C_{16})_2$DTPA adsorbates in a 60:40 ratio.[61,62]

Computational Studies of DDP and DTPA Adsorbates. We performed a computational investigation to gain insight into why DDP and DTPA adsorbates exhibit different binding modes on gold. We substituted ^{n}Bu groups as the aliphatic chains in place of $C_{16}H_{33}$ chains to reduce computational time and cost, and we refer to these model compounds as $(C_4)_2$DDP and $(C_4)_2$DTPA. The model structures were optimized using the B3PW91 DFT method with the basis sets specified in the Experimental Section; pertinent information about the models is presented in Table 1. Comparison of the metrical parameters of the optimized structure of the two anionic ligands reveals that there is very little difference between the two models. For example, the S−P distance of the $(C_4)_2$DTPA$^-$ and $(C_4)_2$DDP$^-$ ligands are very similar to each other (∼1.7% difference) and the S−P−S angles are also very similar (∼1.4% difference). Likewise, the differences between the electronic structure and related properties of these two model systems are also nearly identical. Although the sulfur atoms on the $(C_4)_2$DTPA$^-$ anion bear a more negative charge than those of the oxygenated $(C_4)_2$DDP$^-$ anion, as one would anticipate, the magnitude of this difference is rather small (only ∼0.05 e). The dipole moments along the long axes of $(C_4)_2$DDP and $(C_4)_2$DTPA are oriented toward the headgroup and are identical (10.6 D). The frontier orbital energies for the two anionic models are also quite similar: The $(C_4)_2$DDP$^-$ ligand has a lower HOMO

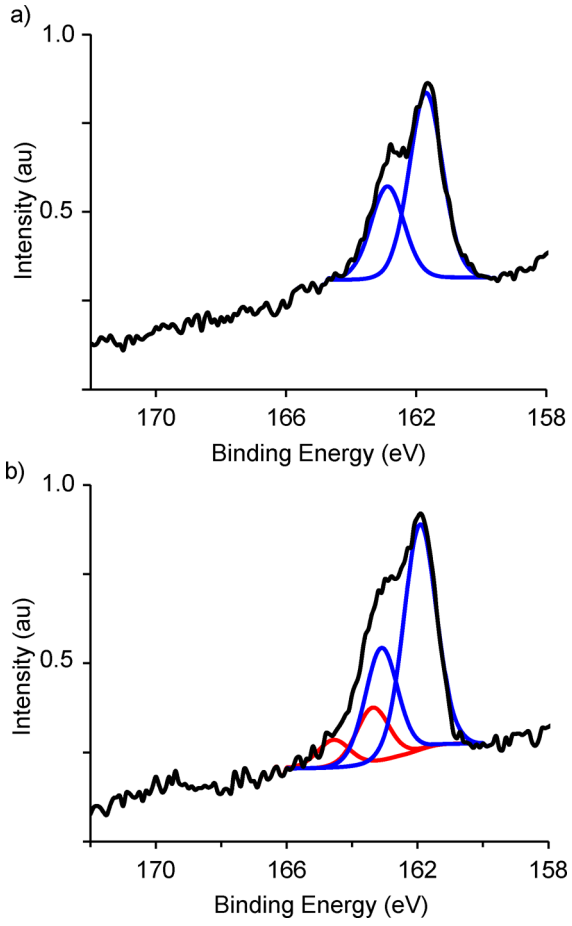

Figure 2. HR-XPS spectra of the S 2p region of (a) $(C_{16})_2$DDP and (b) $(C_{16})_2$DTPA SAMs. The black line corresponds to the experimental spectrum; the blue and red peaks are the fitted S $2p_{3/2}$ and S $2p_{1/2}$ spin−orbit split components of sulfur species bound to gold and noninteracting sulfur species, respectively.

energy than $(C_4)_2$DTPA$^-$ by ∼0.2 eV, and the differences between their HOMO−LUMO gaps is only ∼0.2 eV. Furthermore, the composition and appearance of the frontier orbitals corroborate this interpretation in that both the HOMO and LUMO are strikingly similar to each other. It is worth emphasizing that both ligands feature a HOMO with essentially equivalent contributions from both sulfur atoms, indicating that both anionic ligands are capable of binding in a bidentate fashion.

Calculations of the proton and gold affinities of the anions show that complexation to gold is somewhat more favorable for the $(C_4)_2$DTPA ligand than for the $(C_4)_2$DDP ligand; however, the magnitude of the differences in these affinity values calculated for the two model ligands is minimal (∼20−30 kJ mol^{-1}, corresponding to differences of <2% for the proton affinities and <5% for the gold(I) ion affinities). The small magnitude of the differences between the calculated models suggests that none of them is plausible as the determining factor in the different ligand denticities observed experimentally. More importantly, the calculations reveal that the energetic difference between monodentate (Mono) binding of a gold(I) ion and the corresponding bidentate (Chelate) binding is remarkably small, between 13 and 20 kJ mol^{-1} (only 1.7−2.6%) in favor of bidentate binding, for both model anions. Such a small difference in relative binding energies suggests that

dx.doi.org/10.1021/ja404798q | J. Am. Chem. Soc. 2013, 135, 15784−15793

Table 1. Selected Calculated Results for the Models of the $(C_4)_2$DTPA and $(C_4)_2$DDP Ligands[a]

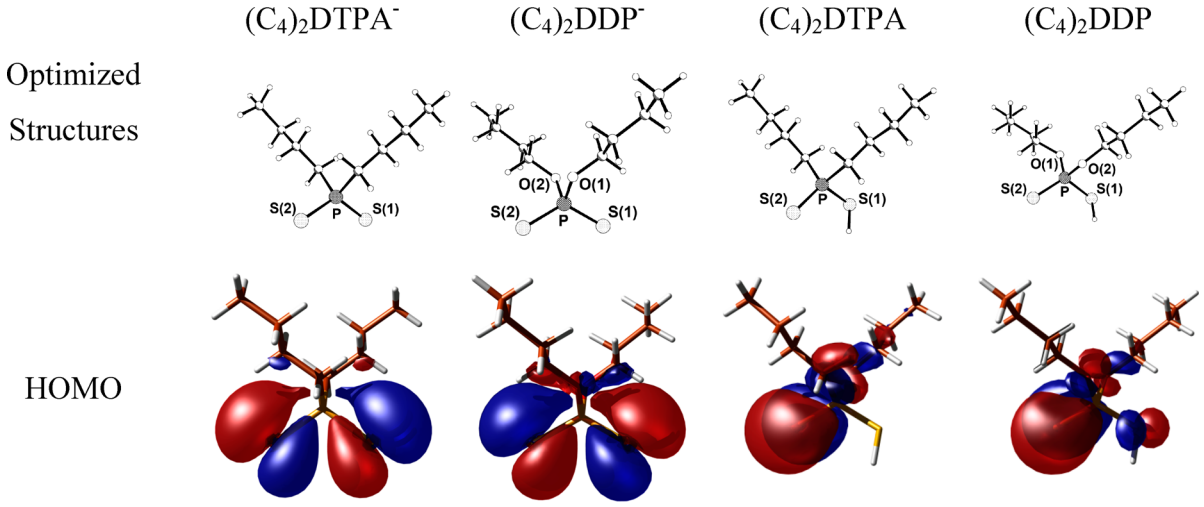

[a]Mono vs chelated describes whether the proton/gold atom is bound by one (Mono) or both (Chelated) of the sulfur centers. Value calculated for the S−P bond of the SH fragment. [b]Natural charge presented in standard atomic units (e).

low-energy interactions between adjacent adsorbates within a SAM (e.g., ion−dipole, dipole−dipole, dispersion forces, etc.) may easily influence whether monodentate or bidentate binding modes are adopted. We note that we simplified the computational work by limiting the study to the binding of a single gold atom. Since the two ligand models interact with a single gold atom (and proton) in an identical fashion, the data provide no rationale for differing binding interactions with an identical surface on the basis of the bonding properties of the ligands.

Perhaps expectedly, examination of the protonated variants of the model ligands also reveals that the differences between these two neutral compounds are minimal: All of the metrical parameters are within 2% of each other. Interestingly, one substantial difference between the two protonated models is observed in the composition of the frontier orbitals. In particular, the HOMO for $(C_4)_2$DTPA lacks any orbital contribution from the sulfur bound to hydrogen, whereas the HOMO in $(C_4)_2$DDP still features a contribution from both sulfur atoms to the MO. The corresponding orbital on $(C_4)_2$DTPA that does feature a contribution from the protonated sulfur center is the HOMO-2 orbital, which is 1.2 eV lower in energy. In spite of this unexpected computational observation, it is unlikely that the difference between the protonated models has any relevance to the experimental results: During sample preparation, any compounds that are physisorbed to the gold surface are rinsed away. Accordingly, the HR-XPS analysis of the S 2p region reveals no evidence that any protonated ligands remain on the surface.

Overall, given that the differences between the calculated properties of these two ligand models are so small, it is most likely that intermolecular interactions (e.g., chain packing, dipole−dipole interactions, etc.) provide the driving force for the observed changes in denticity exhibited by the two ligands. To fully understand these differences, it is necessary to examine and compare the organization of the alkyl chains in $(C_{16})_2$DDP and $(C_{16})_2$DTPA SAMs on As-Dep gold.

Organization of the Alkyl Chains. Along with differences in headgroup binding, $(C_{16})_2$DDP and $(C_{16})_2$DTPA SAMs also exhibit differences in the crystallinity and packing of alkyl chains. RAIR spectra of the methylene C−H stretching region shows the difference in the hexadecyl chain crystallinity of $(C_{16})_2$DDP and $(C_{16})_2$DTPA SAMs (Figure 3). Peak positions are summarized in Table 2. The peak positions of $\nu_{as}(CH_2)$ and

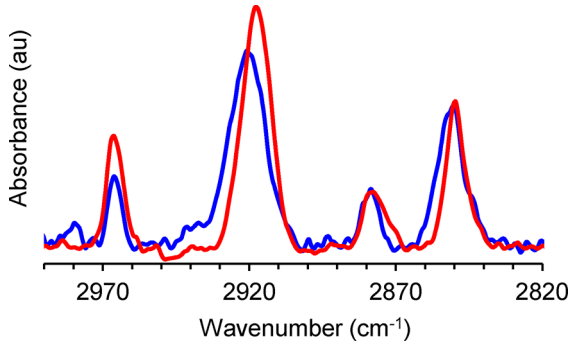

Figure 3. RAIR spectra of C−H stretches region of $(C_{16})_2$DTPA (red) and $(C_{16})_2$DDP (blue) SAMs.

$\nu_s(CH_2)$ of the $(C_{16})_2$DTPA SAM indicate that the SAM is composed of crystalline alkyl groups,[61,62] whereas the $\nu_{as}(CH_2)$ peak position of the $(C_{16})_2$DDP SAM is ~3 cm^{-1} higher. Since $\nu_{as}(CH_2)$ is a more sensitive indicator of alkyl chain crystallinity than $\nu_s(CH_2)$,[83] we conclude that the hexadecyl chains of the $(C_{16})_2$DDP SAM are less crystalline than those of the $(C_{16})_2$DTPA SAM. This conclusion is supported by a comparison of the full width at half-maximum (fwhm) of $\nu_{as}(CH_2)$ and $\nu_s(CH_2)$ peaks. The fwhm of both the $\nu_{as}(CH_2)$ and $\nu_s(CH_2)$ peaks for the $(C_{16})_2$DDP SAM is 3 cm^{-1} larger than that of the $(C_{16})_2$DTPA SAM. The increased fwhm observed for methylene stretching peaks of the $(C_{16})_2$DDP SAM is indicative of heterogeneity in the methylene group orientation, consistent with disorganized, loosely packed alkyl chains.[54]

An analysis of contact angles measured on $(C_{16})_2$DDP and $(C_{16})_2$DTPA SAMs is consistent with the loose alkyl group packing of the former SAM indicated by the RAIRS data. SAMs with loosely packed alkyl groups expose more methylene groups to the probe liquid compared to densely packed SAMs, which present an interface consisting of well-packed methyl groups. SAMs with loosely packed alkyl groups thus have a higher number of interactions between the SAM and the probe

dx.doi.org/10.1021/ja404798q | J. Am. Chem. Soc. 2013, 135, 15784−15793

Table 2. RAIRS Absorption Bands and Contact Angle Data of $(C_{16})_2$DDP and $(C_{16})_2$DTPA SAMs on Gold

SAM	$\nu_{as}(CH_2)$ (cm^{-1})	$\nu_s(CH_2)$ (cm^{-1})	$\nu_{as}(CH_2)$ fwhm (cm^{-1})	$\nu_s(CH_2)$ fwhm (cm^{-1})	$\theta_a(H_2O)$ (°)	θ_a(HD) (°)
$(C_{16})_2$DDP	2921	2850	15	10	111 ± 2	27 ± 2
$(C_{16})_2$DTPA	2918	2850	12	7	107 ± 2	43 ± 2

liquid, which reduces the contact angles.[24] $\theta_a(H_2O)$ of $(C_{16})_2$DDP SAMs is within error of $(C_{16})_2$DTPA SAMs, indicating that water drops cannot distinguish differences in alkyl group packing between the two SAMs. Hexadecane (HD), on the other hand, is more sensitive to alkyl chain packing density. HD interacts with alkyl chains through London dispersion forces, and its low surface tension allows it to intercalate between alkyl chains. The advancing HD contact angle, θ_a(HD) of the $(C_{16})_2$DDP SAM is ~15° lower than that of $(C_{16})_2$DTPA SAM. The loose alkyl group packing of $(C_{16})_2$DDP SAM permits HD to penetrate between the alkyl chains, whereas the $(C_{16})_2$DTPA SAM presents a densely packed methyl group surface that prevents such intercalation.

Electrochemical Barrier Properties. Electrochemical impedance spectroscopy (EIS) is a sensitive method to probe differences in the organization of alkyl chains of SAMs. The resistance of a SAM to the diffusion of a redox probe (an aqueous $K_4Fe(CN)_6/K_3Fe(CN)_6$ solution) to the underlying metal surface is strongly correlated to both the packing density and the presence of defects in SAMs.[27,28] The EIS experiment yields the complex impedance of the SAM by applying a sinusoidal ac perturbation and measuring the current response. Fitting an appropriate circuit model to the impedance data yields values for the resistance (R_{SAM}) and the capacitance (C_{SAM}) of the SAM. C_{SAM} is inversely proportional to the SAM thickness using the equation:[83]

$$d_{SAM} = \frac{\varepsilon\varepsilon_0}{C_{SAM}}$$

where ε is the SAM dielectric constant (as measured for C_nSH SAMs (n = 16, 18) on gold using surface plasmon resonance to be 2.1[84] and ε_0 is the permittivity of free space (8.854×10^{-12} $F \cdot m^{-1}$).

The impedance data of $(C_{16})_2$DDP and $(C_{16})_2$DTPA SAMs are presented in Figure 4 as Bode magnitude plots. The low-frequency region of Figure 4 corresponds to the resistance the SAMs provide against diffusion of the redox probe and clearly shows that the loosely packed alkyl groups of the $(C_{16})_2$DDP SAM are an inferior barrier compared to the densely packed alkyl groups of the $(C_{16})_2$DTPA SAM. We used the simple Randles equivalent circuit, which includes a solution resistance ($R_{Solution}$) in series with a parallel coating capacitance (C_{SAM}) and SAM resistance (R_{SAM}), to model the EIS data (Figure 5).

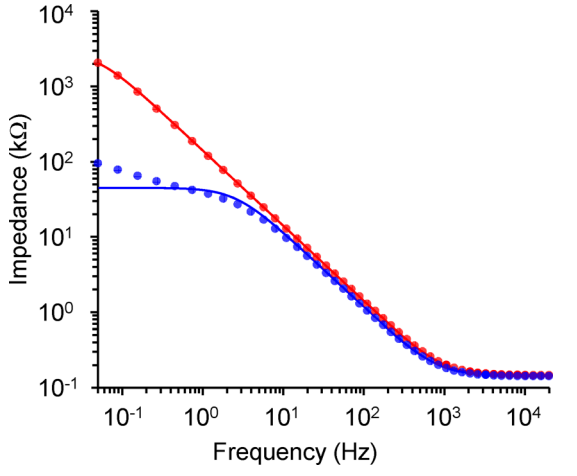

Figure 4. EIS Bode plots of $(C_{16})_2$DTPA (red) and $(C_{16})_2$DDP SAMs (blue). Dots represent measured data, and lines represent the fitted data.

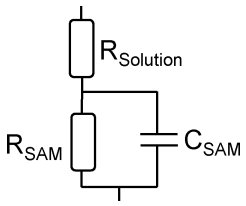

Figure 5. Randles circuit model used to fit EIS data of $(C_{16})_2$DDP and $(C_{16})_2$DTPA SAMs.

Table 3. Resistance, Capacitance and Calculated Monolayer Thickness of $(C_{16})_2$DDP and $(C_{16})_2$DTPA SAMs

adsorbate	resistance (Ω cm^2)	capacitance (μF cm^{-2})	thickness (Å)
$(C_{16})_2$DDP	$4.6 \pm 1.8 \times 10^4$	1.5 ± 0.1	12 ± 1
$(C_{16})_2$DTPA	$2.3 \pm 0.5 \times 10^6$	1.3 ± 0.1	15 ± 1

Table 3 summarizes the resistance and capacitance values from the circuit modeling and the calculated monolayer thickness of $(C_{16})_2$DDP and $(C_{16})_2$DTPA SAMs. $(C_{16})_2$DDP SAMs have a resistance that is 2 orders of magnitude lower than $(C_{16})_2$DTPA SAMs, consistent with a lower packing density of the hexadecyl chains in the former. The $(C_{16})_2$DDP SAM is also slightly thinner than $(C_{16})_2$DTPA SAM, consistent with alkyl groups that are loosely packed and disordered rather than trans-extended and crystalline.

DISCUSSION

$(C_{16})_2$DTPA and the structurally similar adsorbate $(C_{16})_2$DDP both form stable SAMs on As-Dep gold, but with important differences: DTPA SAMs are a mixture of monodentate and bidentate adsorbates and have crystalline alkyl chains, whereas DDP SAMs consist of only bidentate adsorbates and have disorganized alkyl chains. To understand these differences, we considered the hypothesis that an intrinsic difference in either geometric or electronic properties between the two adsorbates could affect the ability of the headgroup to chelate to the As-Dep gold surface. The difference in the percentage of chelating adsorbates in the SAM would then affect the packing of the alkyl chains and give rise to the observed difference in alkyl chain crystallinity. This hypothesis is not supported by the computational study presented herein, which indicates that there are only minor differences in the geometric and electronic properties of DDP and DTPA ligands. These differences are not significant enough to account for the observed differences in chelation. What our calculations did reveal, however, is that the energetic difference between monodentate and bidentate

dx.doi.org/10.1021/ja404798q | J. Am. Chem. Soc. 2013, 135, 15784−15793

binding of a gold(I) ion is remarkably small. This finding contradicts the expectation that chelation will always be highly favored due to the thermodynamic stabilization brought on by the chelate effect. Although chelation is favored for both ligands, the surprisingly small energetic difference means that low-energy interactions between adsorbates may be sufficient to disrupt chelation.

Based on these computational results, we propose that intrinsic differences in chain packing in $(C_{16})_2$DDP and $(C_{16})_2$DTPA SAMs affect whether the adsorbates chelate to the As-Dep gold substrate. Specifically, we suggest that the important difference between $(C_{16})_2$DDP and $(C_{16})_2$DTPA is the greater conformational flexibility of the former due to the P−O−C ether linkage. The well-known conformational flexibility of ether groups in aliphatic ethers arises from the permanent dipole moment of the ether moiety, which promotes gauche conformations over trans by ∼0.1−0.2 kcal mol^{-1}.[85] As a result, inserting an ether linkage into the alkyl chain backbone of *n*-alkanethiolate SAMs on gold, silver,[86] or copper[7] introduces regions of local disorder in the SAM by increasing the population of gauche conformers. The magnitude of the disorder strongly depends on the position of the oxygen atom along the alkyl chain. Positioning the ether group close to either end of the adsorbates (i.e., close to either the methyl tail group or thiolate headgroup) produces the most pronounced disorder.[87] Likewise, the presence of ether groups close to the headgroup of $(C_{16})_2$DDP adsorbates may increase the population of gauche conformers in the SAM to produce the disordered alkyl layer detected by RAIRS and contact angle data. In contrast, $(C_{16})_2$DTPA adsorbates lack ether groups; consequently, SAMs formed from these adsorbates do not exhibit disorder in the organic layer. The chains are trans-extended and pack together via interchain van der Waals interactions to reduce the free energy of the system.

Our hypothesis is that these differences in chain packing affect the ability of the headgroup to chelate to the As-Dep gold surface in $(C_{16})_2$DDP and $(C_{16})_2$DTPA SAMs. We have previously shown that step-edge defects in the deep grain boundaries of As-Dep gold disrupt the chelation of DTPA adsorbates.[61] We concluded that grain boundaries specifically cause this disruption because $(C_{16})_2$DTPA SAMs formed on TS gold, which possesses shallow grain boundaries, consist of adsorbates that are all chelated to the surface. Based on this work, it is reasonable to conclude that the chelation of DDP and DTPA adsorbates on As-Dep gold surfaces also differs specifically at grain boundaries. The present study provides insight into this phenomenon, which is depicted diagrammatically in Scheme 2.[88] The trans-extended alkyl chains of $(C_{16})_2$DTPA SAMs pack into a crystalline arrangement stabilized by interchain van der Waals forces. This crystalline arrangement may prevent the adsorbates from chelating in the deep grain boundaries of As-Dep gold due to steric constraints of the narrow geometry of the grain boundaries. As well, adsorbate binding at the step-edge defects of the grain boundaries may induce an unfavorable orientation that increases the steric hindrance. Instead, monodentate binding may impart the conformational flexibility at the headgroup necessary for the molecules to bind at grain boundaries by allowing rotation about the Au−S bond and small changes in the Au−S−P bond angle, while still maintaining alkyl group packing. Such an arrangement is consistent with the small energy difference between monodentate binding and chelation indicated by the present computational study, which indicates

Scheme 2. Diagram Depicting the Differences in Binding and Alkyl Chain Organization of $(C_{16})_2$DDP and $(C_{16})_2$DTPA Adsorbates at Grain Boundaries on a Gold Surface

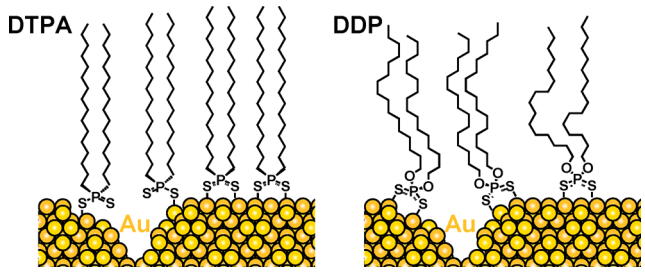

$(C_{16})_2$DTPA adsorbates can adopt monodentate binding without a severe energy penalty. Furthermore, the favorable van der Waals interactions between trans-extended alkyl groups, which have been estimated at ∼2 kcal mol^{-1} per methylene unit,[89] would easily compensate for the small energy difference between monodentate binding and chelation. In contrast, the disorder induced in the alkyl layer of $(C_{16})_2$DDP SAMs by the ether linkages may impart enough conformational flexibility to the alkyl layer to enable these adsorbates to chelate throughout the SAM, even in the sterically constrained spaces of the grain boundaries. Obtaining direct experimental evidence to prove that differences in adsorbate binding are localized at grain boundaries would be immensely challenging; however, the idea that the binding of $(C_{16})_2$DTPA and $(C_{16})_2$DDP adsorbates differs at grain boundaries due to steric constraints (as depicted in Scheme 2) is consistent with the experimental and computational studies presented herein.

It has previously been noted that varying the structure of thiol-containing adsorbates can lead to SAMs on gold with structures that differ from that of *n*-alkanethiolate SAMs.[1] For example, changing from aliphatic to aromatic thiols leads to SAMs in which the adsorbates are slightly less canted,[90−92] leading to the conclusion that the structure of SAMs results from the interplay between the highly favorable interaction of the sulfur-containing headgroup and lateral interactions between the organic groups. Our results take these findings a step further: The interplay driving the self-assembly of adsorbates with S−P−S headgroups not only involves the interaction of the headgroup with the gold surface and interchain interactions but also the morphology of the gold substrate. The combination of all three of these factors—the low-energy difference between monodentate and bidentate binding, the disorder introduced by the ether group, and the specific morphology of the As-Dep gold surface—are what determine headgroup binding and the organization of the organic layer in these SAMs. Synchrotron XPS studies of SAMs formed from the *iso*-amyl derivative of DDP (*i*-Amyl$_2$DDP) on As-Dep gold highlight the complexity of this interplay.[70] These adsorbates form SAMs that incorporate a mixture of monodentate and bidentate adsorbates. It is likely that in these SAMs, the steric demands of the branched *iso*-amyl groups take on a greater importance in determining the SAM structure.

The lower electrochemical barrier properties of the $(C_{16})_2$DDP SAM compared to the $(C_{16})_2$DTPA SAM are a consequence of the disorder imparted by the ether linkage and are consistent with studies comparing the barrier properties of SAMs on copper formed from a series of *n*-alkanethiolates with

dx.doi.org/10.1021/ja404798q | J. Am. Chem. Soc. 2013, 135, 15784−15793

and without ether linkages in the alkyl chains.[7] An EIS study of these SAMs on copper revealed that the resistance of SAMs of *n*-alkanethiolates that incorporate ether groups positioned near the thiolate group significantly reduced the resistance compared to analogous SAMs without the ether linkage, leading to the conclusion that intermolecular interactions between alkyl chains, and not simply alkyl chain length, determines the barrier properties of the SAM. Similar to this study, the barrier properties of $(C_{16})_2$DDP and $(C_{16})_2$DTPA SAMs also highlight the important influence of intermolecular interactions between alkyl chains on electrochemical barrier properties. In these SAMs, it is possible that both interchain interactions and headgroup binding may influence the resistance, and one might expect that chelated head groups would lead to a higher SAM resistance. Despite having chelated head groups, however, the resistance of $(C_{16})_2$DDP SAMs is 2 orders of magnitude lower than that of $(C_{16})_2$DTPA SAMs, which have a mixture of monodentate and chelated head groups. Intermolecular interactions in the organic layer thus overshadow any effect headgroup chelation might have on the barrier properties. The loosely packed, disorganized alkyl chains of the $(C_{16})_2$DDP SAM are a poor electrochemical barrier compared to the well-packed, crystalline alkyl layer of the $(C_{16})_2$DTPA SAM.

CONCLUSIONS

SAMs are an incredibly well-studied area of research; yet, the complexity of the self-assembly process still can be surprising. SAMs with chelating head groups are an emerging field of research due to the beneficial effects of headgroup chelation. Compared to monodentate adsorbates, SAMs formed from chelating adsorbates have improved thermal[24−26] and electrochemical[27−30] stabilities and enhanced electronic coupling to the underlying metal substrate.[56] The robustness of these SAMs makes them more suitable for practical applications, and the possibility of interesting transport properties arising from chelation may eventually place these SAMs at the forefront of molecular junction research. The work presented herein shows that despite the expected thermodynamic stabilization due to the chelate effect, chelation in SAMs may not be a foregone conclusion. The self-assembly process is more complex than expected, and it is the interplay between adsorbate−substrate interactions, intermolecular interactions, and substrate morphology that determines the resulting SAM structure. We believe that understanding this interplay is essential for the development of effective design rules that will one day enable the design of chelating adsorbates that produce complex self-organized structures.

ASSOCIATED CONTENT

Supporting Information

^{31}P, ^{1}H, and ^{13}C NMR spectra of $(C_{16})_2$DDP (Figure S1); XPS survey spectra of $(C_{16})_2$DDP and $(C_{16})_2$DTPA SAMs (Figure S2); details of DFT computations. This material is available free of charge via the Internet at http://pubs.acs.org.

AUTHOR INFORMATION

Corresponding Authors

cmacd@uwindsor.ca
tbcarmic@uwindsor.ca

Notes

The authors declare no competing financial interest.

ACKNOWLEDGMENTS

We dedicate this manuscript to Professor Douglas W. Stephan on the occasion of his 60th birthday. This research was supported by the National Sciences and Engineering Research Council of Canada (NSERC) and by the Ontario Ministry of Research and Innovation through an Early Researcher Award to T.B.C. R.R.S. and C.J.A. are grateful for the award of an Ontario Graduate Scholarship (OGS). We thank Mark Biesinger at Surface Science Western for X-ray photoelectron spectroscopy.

REFERENCES

(1) Love, J. C.; Estroff, L. A.; Kriebel, J. K.; Nuzzo, R. G.; Whitesides, G. M. *Chem. Rev.* **2005**, *105*, 1103−1169.
(2) Laibinis, P. E.; Whitesides, G. M. *J. Am. Chem. Soc.* **1992**, *114*, 9022−9028.
(3) Itoh, M.; Nishihara, H.; Aramaki, K. *J. Electrochem. Soc.* **1995**, *142*, 3696−3704.
(4) Jennings, G. K.; Munro, J. C.; Yong, T.-W.; Laibinis, P. E. *Langmuir* **1998**, *14*, 6130−6139.
(5) Zamborini, F. P.; Crooks, R. M. *Langmuir* **1998**, *14*, 3279−3286.
(6) Jennings, G. K.; Munro, J. C.; Laibinis, P. E. *Adv. Mater.* **1999**, *11*, 1000−1003.
(7) Jennings, G. K.; Yong, T.-H.; Munro, J. C.; Laibinis, P. E. *J. Am. Chem. Soc.* **2003**, *125*, 2950−2957.
(8) Ma, H. Y.; Yang, C.; Yin, B. S.; Li, G. Y.; Chen, S. H.; Luo, J. L. *Appl. Surf. Sci.* **2003**, *218*, 144−154.
(9) Holmlin, R. E.; Haag, R.; Chabinyc, M. L.; Ismagilov, R. F.; Cohen, A. E.; Terfort, A.; Rampi, M. A.; Whitesides, G. M. *J. Am. Chem. Soc.* **2001**, *123*, 5075−5085.
(10) Rampi, M. A.; Whitesides, G. M. *Chem. Phys.* **2002**, *281*, 373−391.
(11) de Boer, B.; Frank, M. M.; Chabal, Y. L.; Jiang, W.; Garfunkel, E.; Bao, Z. *Langmuir* **2004**, *20*, 1539−1542.
(12) Walker, A. V.; Tighe, T. B.; Cabarcos, O. M.; Reinard, M. D.; Heynie, B. C.; Uppili, S.; Winograd, N.; Allara, D. L. *J. Am. Chem. Soc.* **2004**, *126*, 3954−3963.
(13) Wang, W.; Lee, T.; Kretzschumar, I.; Reed, M. A. *Nano Lett.* **2004**, *4*, 643−646.
(14) Akkerman, H. B.; Blom, P. W. M.; de Leeuw, D. M.; de Boer, B. *Nature* **2006**, *441*, 69−72.
(15) Kim, T.-W.; Wang, G.; Lee, H.; Lee, T. *Nanotechnology* **2007**, *18*, 315204−315215.
(16) Weiss, E. A.; Chiechi, R. C.; Kaufman, G. K.; Kriebel, J. K.; Li, Z.; Duati, M.; Rampi, M. A.; Whitesides, G. M. *J. Am. Chem. Soc.* **2007**, *129*, 4336−4349.
(17) Chiechi, R. C.; Weiss, E. A.; Dickey, M. D.; Whitesides, G. M. *Angew. Chem., Int. Ed.* **2008**, *47*, 142−144.
(18) Haick, H.; Cahen, D. *Acc. Chem. Res.* **2008**, *41*, 359−366.
(19) Nijhuis, C. A.; Reus, W. F.; Barber, J. R.; Dickey, M. D.; Whitesides, G. M. *Nano Lett.* **2010**, *10*, 3611−3619.
(20) Thuo, M. M.; Reus, W. F.; Nijhuis, C. A.; Barber, J. R.; Kim, C.; Shulz, M. D.; Whitesides, G. M. *J. Am. Chem. Soc.* **2011**, *133*, 2962−2975.
(21) Wang, G.; Kim, Y.; Choe, M.; Kim, T.-W.; Lee, T. *Adv. Mater.* **2011**, *23*, 755−760.
(22) Chaki, N.; Vijayamohanan, K. *Biosens. Bioelectron.* **2002**, *17*, 1−12.
(23) Frederix, F.; Bonroy, K.; Laureyn, W.; Reekmans, G.; Campitelli, A.; Dehaen, W.; Maes, G. *Langmuir* **2003**, *19*, 4351−4357.
(24) Bain, C. D.; Troughton, E. B.; Tao, Y.-T.; Evall, J.; Whitesides, G. M.; Nuzzo, R. G. *J. Am. Chem. Soc.* **1989**, *111*, 321−335.
(25) Delamarche, E.; Michel, B.; Kang, H.; Gerber, C. *Langmuir* **1994**, *10*, 4103−4108.
(26) Srisombat, L.; Zhang, S.; Lee, T. R. *Langmuir* **2010**, *26*, 41−46.
(27) Yan, D.; Saunders, J. A.; Jennings, G. K. *Langmuir* **2000**, *16*, 7562−7565.

(28) Diao, P.; Guo, M.; Tong, R. *J. Electroanal. Chem.* **2001**, *495*, 98−105.
(29) Yan, D.; Jennings, G. K.; Weinstein, R. D. *Ind. Eng. Chem. Res.* **2002**, *41*, 4528−4533.
(30) Wang, W.; Zhang, S.; Chinwangso, P.; Advincula, R. C.; Lee, T. R. *J. Phys. Chem. C* **2009**, *113*, 3717−3725.
(31) Chinwangso, P.; Jamison, A. C.; Lee, T. R. *Acc. Chem. Res.* **2011**, *44*, 511−519.
(32) Cotton, F. A.; Wilkinson, G.; Murillo, C. A.; Bochmann, M. *Advanced Inorganic Chemistry*, 6th ed.; Wiley-Interscience: Hoboken, NJ, 1999.
(33) Lee, Y. J.; Jeon, I. C.; Park, W.-K.; Kim, K. *Langmuir* **1996**, *12*, 5830−5837.
(34) Garg, N.; Lee, T. R. *Langmuir* **1998**, *14*, 3815−3819.
(35) Kim, C. H.; Han, S. W.; Ha, T. H.; Kim, K. *Langmuir* **1999**, *15*, 8399−8404.
(36) Lim, J. K.; Kim, Y.; Kwon, O.; Joo, S.-W. *ChemPhysChem* **2008**, *9*, 1781−1787.
(37) Lim, J. K.; Kwon, O.; Joo, S.-W. *J. Phys. Chem. C* **2008**, *112*, 6816−6821.
(38) Bruno, G.; Babudri, F.; Operamolla, A.; Bianco, G. V.; Losurdo, M.; Giangregorio, M. M.; Omar, O. H.; Mavelli, F.; Farinola, G. M.; Capezzuto, P.; Naso, F. *Langmuir* **2010**, *26*, 8430−8440.
(39) Fox, M. A.; Whitesell, J. K.; McKerrow, A. J. *Langmuir* **1998**, *14*, 816−820.
(40) Kittredge, K. W.; Minton, M. A.; Fox, M. A.; Whitesell, J. K. *Helv. Chim. Acta* **2002**, *85*, 788−798.
(41) Yam, C. M.; Cho, J.; Cai, C. *Langmuir* **2003**, *19*, 6862−6868.
(42) Park, J.-S.; Vo, A. N.; Barriet, D.; Shon, Y.-S.; Lee, T. R. *Langmuir* **2005**, *21*, 2902−2911.
(43) Kitagawa, T.; Idomoto, Y.; Matsubara, H.; Hobara, D.; Kakiuchi, T.; Okazaki, T.; Komatsu, K. *J. Org. Chem.* **2006**, *71*, 1362−1369.
(44) Katano, S.; Kim, Y.; Matsubara, H.; Kitagawa, T.; Kawai, M. *J. Am. Chem. Soc.* **2007**, *129*, 2511−2515.
(45) Shon, Y.-S.; Lee, T. R. *Langmuir* **1999**, *15*, 1136−1140.
(46) Shon, Y.-S.; Lee, S.; Perry, S. S.; Lee, T. R. *J. Am. Chem. Soc.* **2000**, *122*, 1278−1281.
(47) Shon, Y.-S.; Lee, S.; Colorado, R., Jr.; Perry, S. S.; Lee, T. R. *J. Am. Chem. Soc.* **2000**, *122*, 7556−7563.
(48) Shon, Y.-S.; Lee, T. R. *J. Phys. Chem. B* **2000**, *104*, 8192−8200.
(49) Shon, Y.-S.; Colorado, R., Jr.; Williams, C. T.; Bain, C. D.; Lee, T. R. *Langmuir* **2000**, *16*, 541−548.
(50) Lee, S.; Shon, Y.-S.; Colorado, R., Jr.; Guenard, R. L.; Lee, T. R.; Perry, S. S. *Langmuir* **2000**, *16*, 2220−2224.
(51) Park, J.-S.; Smith, A. C.; Lee, T. R. *Langmuir* **2004**, *20*, 5829−5836.
(52) Zhao, Y.; Pérez-Segarra, W.; Shi, Q.; Wei, A. *J. Am. Chem. Soc.* **2005**, *127*, 7328−7329.
(53) Morf, P.; Raimondi, F.; Nothofer, H.-G.; Schnyder, B.; Yasuda, A.; Wessels, J. M.; Jung, T. A. *Langmuir* **2006**, *22*, 658−663.
(54) Weinstein, R. D.; Richards, J.; Thai, S. D.; Omiatek, D. M.; Bessel, C. A.; Faulkner, C. J.; Othman, S.; Jennings, G. K. *Langmuir* **2007**, *23*, 2887−2891.
(55) Zhu, H.; Coleman, D. M.; Dehen, C. J.; Geisler, I. M.; Zemlyanov, D.; Chmielewski, J. C.; Simpson, G. J.; Wei, A. *Langmuir* **2008**, *24*, 8660−8666.
(56) von Wrochem, F.; Gao, D.; Scholz, F.; Nothofer, H.-G.; Nelles, G.; Wessels, J. M. *Nat. Nanotechnol.* **2010**, *5*, 618−624.
(57) Gao, D.; Scholz, F.; Nothofer, H.-G.; Ford, W. E.; Scherf, U.; Wessels, J. M.; Yasuda, A.; von Wrochem, F. *J. Am. Chem. Soc.* **2011**, *133*, 5921−5930.
(58) Colorado, R., Jr.; Villazana, R. J.; Lee, T. R. *Langmuir* **1998**, *14*, 6337−6340.
(59) Lee, T.-C.; Hounihan, D. J.; Colorado, R., Jr.; Park, J.-S.; Lee, T. R. *Phys. Chem. B* **2004**, *108*, 2648−2653.
(60) Lee, T.-C.; Chen, P.-C.; Lai, T.-Y.; Tuntiwechapikul, W.; Kim, J.-H.; Lee, T. R. *Appl. Surf. Sci.* **2008**, *254*, 7064−7068.
(61) Miller, M. S.; San Juan, R. R.; Ferrato, M.-A.; Carmichael, T. B. *Langmuir* **2011**, *27*, 10019−10026.
(62) San Juan, R. R.; Miller, M. S.; Ferrato, M.-A.; Carmichael, T. B. *Langmuir* **2012**, *28*, 13253−13260.
(63) Gupta, P.; Loos, K.; Korniakov, A.; Spagnoli, C.; Cowman, M. K.; Ulman, A. *Angew. Chem., Int. Ed.* **2004**, *43*, 520−523.
(64) Gupta, P.; Ulman, A.; Fanfan, S.; Korniakov, A.; Loos, K. *J. Am. Chem. Soc.* **2005**, *127*, 4−5.
(65) Nijhuis, C. A.; Reus, W. F.; Whitesides, G. M. *J. Am. Chem. Soc.* **2009**, *131*, 17814−17827.
(66) Nijhuis, C. A.; Reus, W. F.; Whitesides, G. M. *J. Am. Chem. Soc.* **2010**, *132*, 18386−18401.
(67) Fracasso, D.; Valkenier, H.; Hummelen, J. C.; Solomon, G. C.; Chiechi, R. C. *J. Am. Chem. Soc.* **2011**, *133*, 9556−9563.
(68) Hope, G. A.; Woods, R.; Watling, K. *Colloids Surf., A* **2003**, *214*, 87−97.
(69) Hicyilmaz, C.; Altun, N. E. *J. Appl. Electrochem.* **2006**, *36*, 609−616.
(70) Beattie, D. A.; Kempson, I. M.; Fan, L.-J.; Skinner, W. M. *Int. J. Miner. Process.* **2009**, *92*, 162−168.
(71) Persson, N.-O.; Uvdal, K.; Almquist, O.; Engquist, I.; Kariis, H.; Liedberg, B. *Langmuir* **1999**, *15*, 8161−8169.
(72) Gümgüm, B.; Biricik, N.; Baysal, A. *Phosphorus, Sulfur and Silicon* **2000**, *167*, 111−116.
(73) Horcas, I.; Fernandez, R.; Gomez-Rodriguez, J. M.; Colchero, J.; Gomez-Herrero, J.; Baro, A. M. *Rev. Sci. Instrum.* **2007**, *78*, 013705.
(74) Moulder, J. F.; Stickle, W. F.; Sobol, P. E.; Bomben, K. D. *Handbook of X-Ray Photoelectron Spectroscopy*; Physical Electronics: Eden Prairie, MN, 1995.
(75) Frisch, M. J.; Trucks, G. W.; Schlegel, H. B.; Scuseria, G. E.; Robb, M. A.; Cheeseman, J. R.; Scalmani, G.; Barone, V.; Mennucci, B.; Petersson, G. A.; Nakatsuji, H.; Caricato, M.; Li, X.; Hratchian, H. P.; Izmaylov, A. F.; Bloino, J.; Zheng, G.; Sonnenberg, J. L.; Hada, M.; Ehara, M.; Toyota, K.; Fukuda, R.; Hasegawa, J.; Ishida, M.; Nakajima, T.; Honda, Y.; Kitao, O.; Nakai, H.; Vreven, T.; Montgomery, J. A., Jr.; Peralta, J. E.; Ogliaro, F.; Bearpark, M.; Heyd, J. J.; Brothers, E.; Kudin, K. N.; Staroverov, V. N.; Kobayashi, R.; Normand, J.; Raghavachari, K.; Rendell, A.; Burant, J. C.; Iyengar, S. S.; Tomasi, J.; Cossi, M.; Rega, N.; Millam, N. J.; Klene, M.; Knox, J. E.; Cross, J. B.; Bakken, V.; Adamo, C.; Jaramillo, J.; Gomperts, R.; Stratmann, R. E.; Yazyev, O.; Austin, A. J.; Cammi, R.; Pomelli, C.; Ochterski, J. W.; Martin, R. L.; Morokuma, K.; Zakrzewski, V. G.; Voth, G. A.; Salvador, P.; Dannenberg, J. J.; Dapprich, S.; Daniels, A. D.; Farkas, Ö.; Foresman, J. B.; Ortiz, J. V.; Cioslowski, J.; Fox, D. J. *Gaussian 09*, C.1, Gaussian, Inc.: Wallingford, CT, 2009
(76) Dolg, M.; Wedig, U.; Stoll, H.; Preuss, H. *J. Chem. Phys.* **1987**, *86*, 866−872.
(77) Schwerdtfeger, P.; Dolg, M.; Schwartz, W. H. E.; Bowmaker, G. A.; Boyd, P. D. W. *J. Chem. Phys.* **1989**, *91*, 1762−1774.
(78) Reed, A. E.; Curtiss, L. A.; Weinhold, F. *Chem. Rev.* **1988**, *88*, 899−926.
(79) Schaftenaar, G.; Noordik, J. H. *J. Comput.-Aided Mol. Des.* **2000**, *14*, 123−134.
(80) Cason, C.; Froehlich, T.; Kopp, N.; Parker, R. *Persistence of Vision Raytracer (POV-Ray) for Windows, 3.6*; Persistence of Vision Raytracer Pty. Ltd.: Victoria, Australia, 2009.
(81) Castner, D. G.; Hinds, K.; Grainger, D. W. *Langmuir* **1996**, *12*, 5083−5086.
(82) Ishida, T.; Choi, N.; Mizutani, W.; Tokumoto, H.; Kojima, I.; Azehara, H.; Hokari, H.; Akiba, U.; Fujihira, M. *Langmuir* **1999**, *15*, 6799−6806.
(83) Porter, M. D.; Bright, T. B.; Allara, D. L.; Chidsey, C. E. D. *J. Am. Chem. Soc.* **1987**, *109*, 3559−3568.
(84) Peterlinz, K. A.; Georgiadis, R. *Langmuir* **1996**, *12*, 4731−4740.
(85) Miwa, Y.; Machida, K. *J. Am. Chem. Soc.* **1989**, *111*, 7733−7739.
(86) Laibinis, P. E.; Bain, C. D.; Nuzzo, R. G.; Whitesides, G. M. *J. Phys. Chem.* **1995**, *99*, 7663−7676.
(87) Srivastava, P.; Chapman, W. G.; Laibinis, P. E. *Langmuir* **2009**, *25*, 2869−2695.
(88) In Scheme 2, the adsorbate bond lengths and spacing of the gold lattice are not drawn to scale and are not meant to imply how the

adsorbates bind relative to the gold lattice; rather, we use this scheme simply to illustrate the differences between $(C_{16})_2$DTPA and $(C_{16})_2$DDP binding at grain boundaries.
(89) Sellers, H.; Ulman, A.; Shnidman, Y.; Eilers, J. E. *J. Am. Chem. Soc.* **1993**, *115*, 9389−9401.
(90) Geyer, W.; Stadler, V.; Eck, W.; Zharnikov, M.; Gölzhäuser, A.; Grunze, M. *Appl. Phys. Lett.* **1999**, *75*, 2401−2403.
(91) Frey, S.; Stadler, V.; Heister, K.; Eck, W.; Zharnikov, M.; Grunze, M. *Langmuir* **2001**, *17*, 2408−2415.
(92) Ulman, A. *Acc. Chem. Res.* **2001**, *34*, 855−863.